Self-Limited Growth of a Thin Oxide Layer on Rh(111)

J. Gustafson,[1,*] A. Mikkelsen,[1] M. Borg,[1] E. Lundgren,[1] L. Köhler,[2] G. Kresse,[2] M. Schmid,[3] P. Varga,[3] J. Yuhara,[4] X. Torrelles,[5] C. Quirós,[6,†] and J. N. Andersen[1]

[1]*Department of Synchrotron Radiation Research, Lund University, Box 118, S-221 00, Sweden*
[2]*Institut für Materialphysik and Centre for Computational Materials Science, Universität Wien, A-1090 Wien, Austria*
[3]*Institut für Allgemeine Physik, Technische Universität Wien, A-1040 Wien, Austria*
[4]*Department of Physical Science and Engineering, Nagoya University, Nagoya, 464-8603, Japan*
[5]*Institut de Ciencia de Materials de Barcelona (C.S.I.C), 08193, Bellaterra, Barcelona, Spain*
[6]*European Synchrotron Radiation Facility, BP 220, 38043 Grenoble CEDEX, France*

(Received 4 November 2003; published 26 March 2004)

The oxidation of the Rh(111) surface at oxygen pressures from 10^{-10} mbar to 0.5 bar and temperatures between 300 and 900 K has been studied on the atomic scale using a multimethod approach of experimental and theoretical techniques. Oxidation starts at the steps, resulting in a trilayer O-Rh-O surface oxide which, although not thermodynamically stable, prevents further oxidation at intermediate pressures. A thick corundum like Rh_2O_3 bulk oxide is formed only at significantly higher pressures and temperatures.

DOI: 10.1103/PhysRevLett.92.126102 PACS numbers: 68.35.Bs, 68.37.Ef, 68.47.Gh, 68.43.Bc

Oxidation is often associated with corrosion, but under the right conditions it can lead to oxide layers which can be applied, e.g., as protective layers against corrosion, as insulating layers in microelectronic devices, and as catalytic devices [1,2]. To obtain optimal properties for an oxide layer aimed at a particular purpose, knowledge is required on the fundamental oxidation processes, such as the reactions at the surface and at the metal-oxide interface and the transport of species through the oxide layers. In recent years, this importance has been recognized and, as a consequence, significant attempts have been made to study the initial oxidation of clean and well prepared surfaces under ultrahigh vacuum (UHV) conditions experimentally and theoretically [3–9]. For late transition metals and noble metals (e.g., Pd and Ag), it is now understood that oxidation proceeds through ultrathin oxide layers, which are *thermodynamically stable* at intermediate oxygen potentials and can exhibit astonishing complexity [7–10]. It is unclear whether the same holds for transition metals further to the left in the periodic table, whether ultrathin oxide layers different from the bulk oxide exist on these metals and, if so, whether they are only metastable, transient precursors in the form of subsurface oxygen as suggested in a recent theoretical study [4]. It is also unknown whether metastable ultrathin oxide layers can be stabilized by mechanisms other than simple diffusion barriers. To answer these questions, we demonstrate here experimentally that well ordered ultrathin oxide layers can be prepared on Rh(111), similar to Ag and Pd(111). Extensive density functional theory (DFT) calculations for thin RhO films using realistic models and varying thickness reveal that (i) the bulk Rh_2O_3 oxide is thermodynamically more stable than ultrathin layers, and (ii) two and three layer thick oxide films form an effective kinetic barrier towards bulk oxide formation. Additionally, we demonstrate that it is now possible to follow, with atomic resolution, the oxygen interaction and oxidation of a metal surface in a pressure range from 10^{-10} mbar to 0.5 bar by a combination of several experimental and theoretical techniques, which we consider a key development for further studies.

High resolution core level photoelectron spectroscopy (HRCLS) measurements were done at beam line I311 at MAX II in Lund, Sweden [11]. Scanning tunneling microscopy (STM) measurements were done in Vienna at room temperature using the same instrument as in Ref. [8]. Surface x-ray diffraction (SXRD) measurements were carried out at the ID3 surface diffraction beam line [12] at the ESRF (Grenoble, France). The crystal basis used to describe the (H, K, L) diffraction is a hexagonal basis $(\mathbf{a}_1, \mathbf{a}_2, \mathbf{a}_3)$, with $\mathbf{a}_1$ and $\mathbf{a}_2$ in the surface plane with equal distance $[a_0/\sqrt{2}, a_0(\mathrm{Rh}) = 3.80$ Å] and $\mathbf{a}_3$ perpendicular to the surface $(a_0 \times \sqrt{3})$. In all cases, the Rh(111) surface was cleaned using standard cleaning methods. Density functional calculations used the Vienna *ab initio* simulation package (VASP) [13], employing the projector-augmented wave method [14] with a plane wave cutoff of 250 eV and generalized gradient corrections [15]. The Rh substrate was modeled by four layer thick slabs, using (8×8) k points in the Brillouin zone of the primitive surface cell.

The initial exposure of the Rh(111) substrate to oxygen does not reveal any peculiarities. As the amount of oxygen is increased, it gradually covers the entire surface forming a series of structures $[p(2 \times 2),(2 \times 1)$, and $(2\sqrt{3} \times 2\sqrt{3})R30°]$ with oxygen coverages of 0.25, 0.5, and 0.66 ML, respectively [16]. However, at an oxygen partial pressure of around 2×10^{-4} mbar and sample temperature of 800 K, the formation of a Rh surface oxide is observed (Fig. 1), similar to other late transition metals [5,7,8]. The STM image in Fig. 1(a) indicates that, for surface oxide formation on Rh(111), the structure

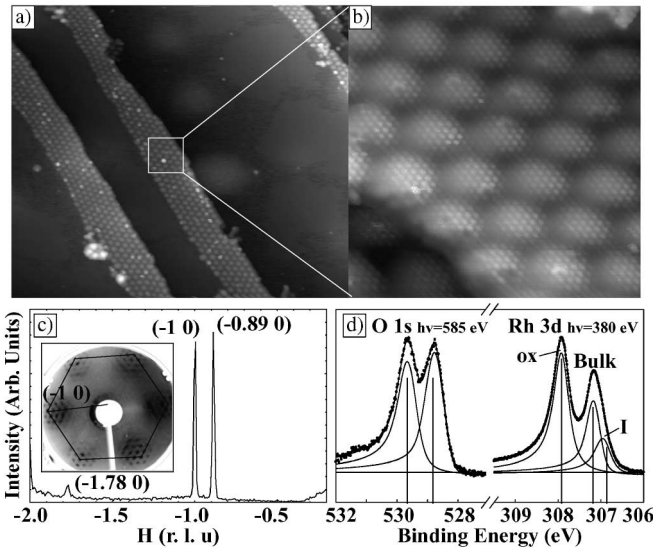

FIG. 1. (a) STM image ($V_{\text{sample}} = -0.6$ V, 0.5 nA, 100×100 nm^2) of the Rh(111) surface exposed to 2×10^{-4} mbar O_2 for 60 s at 650 K. (b) STM image (-4 mV, 0.5 nA, 10×10 nm^2). (c) SXRD H scan at $K = 0$ and $L = 0.3$ as indicated by the black line in the inset of the LEED pattern. (d) HRCLS of O 1s and Rh 3$d_{5/2}$. Vertical lines indicate the calculated peak shifts. In (c) and (d), the Rh(111) surface is exposed to 10^{-3} mbar O_2 for 600 s at 800 K, resulting in a closed oxide film.

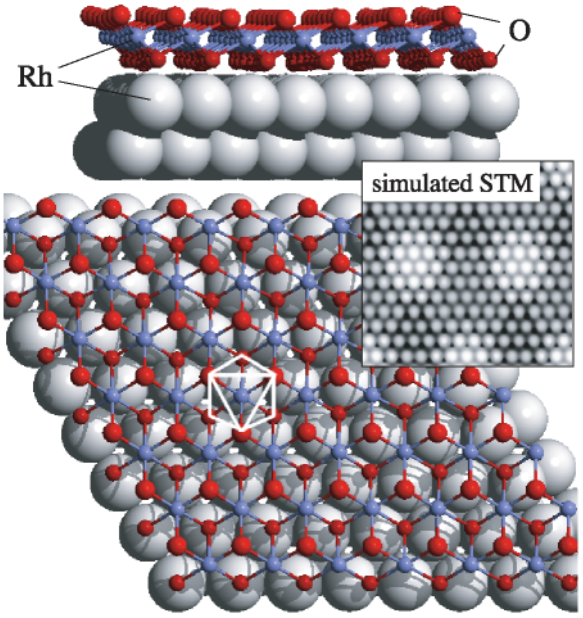

FIG. 2 (color online). Side and top views of the most stable Rh surface oxide as calculated by DFT (octahedrally coordinated Rh atom is indicated). The inset shows the STM simulation using the Tersoff-Hamann approach [18] (filled states between -0.6 and 0 eV).

starts to grow at steps. The reason for this is most likely that oxygen can penetrate at steps more easily into the bulk than on terraces. The in-plane lattice constant of the Rh surface oxide and the composition can be deduced from the data shown in Figs. 1(b)–1(d). In Fig. 1(b), an STM image displaying bright protrusions spaced by 3 Å can be seen. The long range undulation with a periodicity of 7–8 bright spots is easily explicable as a moiré pattern due to the misfit between the surface lattice observed and the in-plane Rh(111) interatomic distance of 2.69 Å. This is substantiated by the LEED pattern shown in Fig. 1(c). The black hexagon connects the diffraction peaks of the Rh(111) surface. The additional spots result from the moiré pattern. The in-plane lattice distance of the Rh oxide is determined precisely as 3.02 Å by SXRD [Fig. 1(c)]. Thus, the lattice can be described as an (8×8) hexagonal Rh oxide on a (9×9) Rh(111) surface unit cell. The composition of the surface oxide can be estimated from the number of components in the O 1s and Rh 3$d_{5/2}$ core levels found by HRCLS [Fig. 1(d)], indicating two different O species as well as one highly O coordinated Rh species (marked "ox") and most likely a Rh interface peak (marked "I").

Inspired by Ref. [17], a trilayer oxide consisting of hexagonal layers of O, Rh, and O again was adsorbed on the Rh(111) substrate and relaxed using DFT. In the DFT calculations, (7×7) O-Rh-O unit cells on an (8×8) Rh(111) surface supercell [$RhO_2(7 \times 7)$@$Rh(8 \times 8)$], as shown in Fig. 2, were found to be more stable than the $RhO_2(8 \times 8)$@$Rh(9 \times 9)$ structure, probably because the ratio of the theoretical lattice constants of a freestanding hexagonal O-Rh-O layer and the Rh substrate is $a_{\text{O-Rh-O}}/a_{\text{Rh}} = 3.10/2.72 \approx 8/7$ in DFT. As discussed below, this particular trilayer structure is the most favorable surface oxide under certain conditions. The simulated STM image (inset of Fig. 2) agrees well with experiment and indicates that the bright spots correspond to the outermost oxygen atoms in the surface oxide. The long range undulations stem from the alignment of the interfacial oxygen atoms, with darker areas corresponding to interfacial oxygen atoms above the Rh hollow sites. At those sites, the binding and the orbital overlap between the metal and the oxide is rather weak resulting in a small tunneling probability. The calculated Rh 3d core binding energy shifts, shown in Fig. 1(d), are in excellent agreement with experiment. In DFT the core level shifts, including final state effects, are 0.78 and -0.32 eV for the Rh atoms in the oxide and at the interface, respectively (experiment 0.79 and -0.22). The oxygen 1s core levels split by 0.84 eV in DFT compared to 0.91 in experiment, with the oxygen at the interface having the larger binding energy. Furthermore, the trilayer is confirmed by a structural analysis of in-plane and out-of-plane structure factors obtained by SXRD.

We now turn to the details of the calculations for the structural determination of the considered trilayer. First, it is noted that a surface oxide with a periodicity of 3.02 Å is not expected on the grounds of the bulk Rh_2O_3 corundum structure. To determine candidates for the ultrathin oxide, we therefore had to resort to an extensive search of configuration space. This would have been impossible for

the experimentally observed lattice with its huge unit cell, but a similar lattice match can be realized in a much smaller supercell by placing a $(\sqrt{3} \times \sqrt{3})R30°$ oxide overlayer on a (2×2) Rh surface unit cell [see Fig. 3(b)]. Additionally, the same supercell can be applied to model the formation of bulk Rh_2O_3 on Rh(111), since Rh_2O_3 has a lattice constant of $a = 5.127$ Å (theory: $a = 5.21$ Å) in the basal plane, which is approximately twice the in-plane lattice constant of the Rh(111) substrate (experiment: $a = 2.69$ Å; theory: $a = 2.72$ Å). Using this comparatively cheap setup, we performed an extensive search of configuration space starting from the corundum Rh_2O_3 lattice. The oxygen atoms were placed at the positions of the oxygen sublattice of the corundum structure allowing only local relaxation but no change in the stacking sequence—a reasonable approximation, since the electrostatic repulsion between the oxygen atoms is minimized in this structure. Thin oxides with 2–4 oxygen layers were considered. Between each oxygen layer, one, two, or three Rh atoms were placed at the octahedral sites and the structures were optimized. Additionally, for two oxygen layers, the search was extended to structures with a tetrahedral Rh coordination in the oxide as suggested for Al_2O_3 on Al(111) [20].

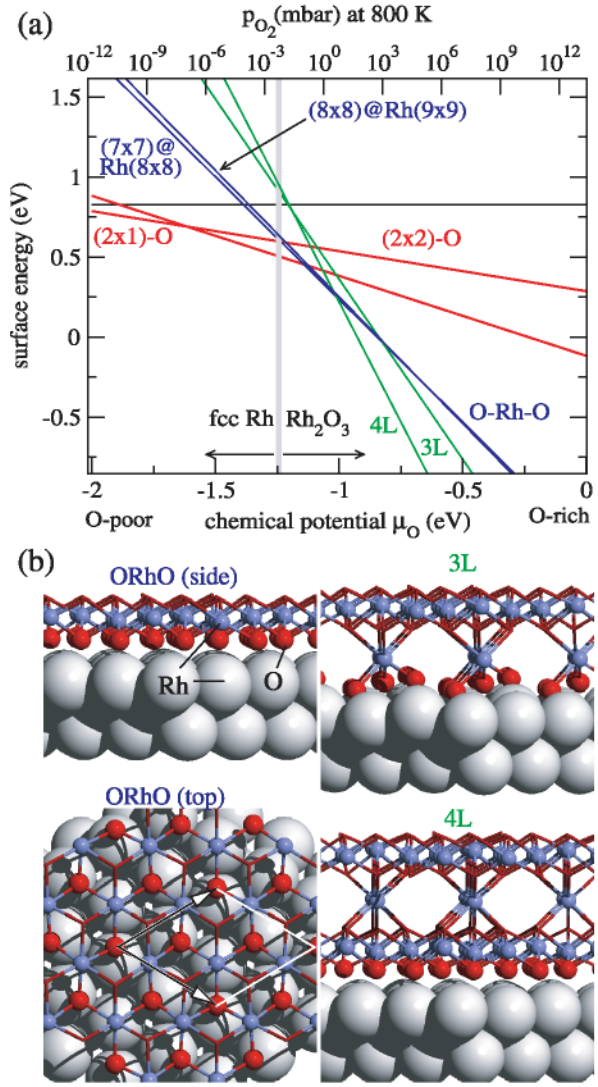

FIG. 3 (color online). (a) Calculated phase diagram and (b) lowest energy structures for oxides with 2 (O-Rh-O), 3, and 4 layers (L) of oxygen on a Rh(111) (2×2) supercell. Oxygen atoms are not shown as balls, but bonds only, except for the bottom oxygen layer. The chemical potential is related to the temperature and the oxygen partial pressure p through the ideal gas equation $\mu_O(T, p) = \mu_O(T, p^0_O) + 1/2 k_B T \ln(p/p^0)$ [19].

The final surface phase diagram is shown in Fig. 3(a), and the most favorable structures for 2, 3, and 4 oxygen layers for the (2×2) supercell are depicted in Fig. 3(b). Results for the large supercell calculations limited to two oxygen layers are included in the phase diagram as well [Rh(8 × 8) and Rh(9 × 9)]. For two oxygen layers, the hexagonal trilayer is indeed found to be most stable with almost identical surface energies for $RhO_2(\sqrt{3} \times \sqrt{3})$@Rh(2 × 2), $RhO_2(7 \times 7)$@Rh(8 × 8), and $RhO_2(8 \times 8)$@Rh(9 × 9), indicating only weak strain effects. In contrast to oxygen atoms on the clean metal, the oxygen atoms at the oxide/metal interface are located preferentially on top of the surface Rh atoms (shifted slightly towards the bridge site), which agrees with previous studies for VO_x and PdO_x on Pd [3,8]. Remarkably, the trilayer termination remains favorable even for thicker oxides. For three oxygen layers ($3L$), the topmost surface layer contains three Rh atoms, and a fourth single Rh atom is located in the second oxide layer. For four oxygen layers ($4L$), the trilayer is found at both sides of the oxide, and a single Rh atom interlinks the two O-Rh-O layers. This pattern continues to the (0001) surface of bulk corundum Rh_2O_3, where the favorable termination is found to be the same type of sparse Rh layer plus trilayer, resulting in a stacking of Rh_2-O_3-Rh-O_3-Rh_3-O_3.

Experimentally, the structure and morphology of the surface and the surface oxide does not change as the O_2 pressure is increased to 1×10^{-3} mbar. The oxidation at O_2 partial pressures above 10^{-3} mbar is beyond the pressure range of standard UHV experiments. The structural development at higher pressures was therefore studied by SXRD, which allowed us to measure *at* these O_2 pressures and elevated temperatures. Figure 4(a) shows the development of the H scan at a sample temperature of 800 K. At an O_2 pressure of 10 mbar, a new component appears at −0.91 reciprocal lattice units (r.l.u.) and grows with increasing O_2 pressure, indicating that a thicker Rh_2O_3 corundum-type oxide starts growing. This suggestion is confirmed by corresponding out-of-plane scans [Fig. 4(b)] where we observe an increasing intensity at $L = 1.43$ and $L = 2.86$ corresponding to scattering from the (0001) planes of corundum Rh_2O_3 (distance 2.308 Å).

To continue the growth to a thick bulklike oxide (see inset of Fig. 4), even higher temperatures are required (900 K), probably because diffusion in the already existing oxidized surface is inhibited at lower temperatures. A

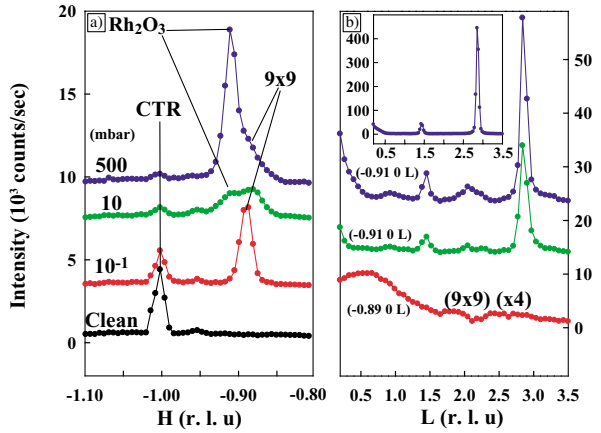

FIG. 4 (color online). *In situ* high-pressure SXRD measurements demonstrating oxidation finally leading to bulklike Rh_2O_3. (a) H scan with $K = 0$ and $L = 0.3$ at O_2 pressures from 10^{-1} mbar to 0.5 bar at 800 K sample temperature. Note the shift from $H = -0.89$ to $H = -0.91$ as the bulk Rh_2O_3 starts to grow. (b) The corresponding out-of-plane scans show the growth of Rh_2O_3 bulk oxide from the (9×9) surface oxide resulting in peaks at $= 1.43$ and $L = 2.86$ r.l.u. Inset: Out-of-plane scan of a thick Rh_2O_3 film prepared at 900 K and 100 mbar O_2.

detailed inspection of reciprocal space confirms that the orientation and geometry of this film is $Rh_2O_3(0001) \parallel Rh(111)$ with the same azimuthal orientation as the trilayer oxide $[Rh_2O_3(11\bar{2}0) \parallel Rh(11\bar{2})]$. The fact that we are able to observe the coexistence of the (9×9) and the Rh_2O_3 film in a large pressure range (10–500 mbar) indicates a kinetic hindrance.

These experimental observations can be understood from the calculated energetic considerations. Our results presented in Fig. 3(a) indicate that a single oxygen trilayer on Rh(111) is in fact only metastable, as the trilayer forms only under conditions where bulk Rh_2O_3 is already stable (to the right of the thick grey line in Fig. 3, experimental value -1.19 eV). Hence, the trilayer is only *kinetically* stabilized, contrary to the situation on Pd(111) where a Pd_5O_4 adlayer is *thermodynamically* stable for intermediate oxygen potentials [8]. An important hint to the reason of the kinetic stability of the O-Rh-O trilayer is given by the results for the three and four layer thick oxides. Four (three) layer oxides have a lower stability than the single trilayer for oxygen potentials $\mu_O < -0.99$ eV ($\mu_O < -0.78$ eV) corresponding to 10 mbar (1 bar) at 800 K. The formation of the bulk oxide must however proceed through thicker oxide layers, which presents a kinetic barrier for the formation of the bulk oxide at too low chemical potentials. Only at sufficiently high pressures is this barrier surmountable, and transformation to the corundum structure is attainable.

In summary, we have characterized the oxidation of a well-defined single crystal metal surface on the atomic scale. As an intermediate structure a hexagonal RhO_2 surface oxide trilayer is observed, which under proper conditions is kinetically stable, since significant barriers inhibit further growth (self-limited oxidation). Similar trilayers have been observed on other surfaces, for instance, VO_x on Pd(111) [3] and RhO_2/Rh(100). It is tempting to conclude that hexagonal trilayer structures are favorable transient structures occurring during the oxidation of metals, and that these structures, under certain conditions, act as a protective layer preventing further oxidation.

The present study also continues the 4*d* series from Ag, over Pd to Rh. On Ag(111) the surface oxide is thermodynamically stable for a fairly large range of oxygen potentials (0.25 eV, Ref. [9]) whereas for Pd its stability regime is narrower (0.15 eV, Ref. [8]), and finally for Rh the surface oxide is only a transient, kinetically stabilized structure. This trend suggests that oxidation via ultrathin stable or metastable surface oxides is specific to the late transition metals and noble metals.

This work was financially supported by the Swedish Research Council, the Austrian FWF, and the Spanish MCyT (MAT2002-02808). Support by the MAX-lab staff is gratefully acknowledged. The computations were performed on Schrödinger II at the computing center of the University Vienna.

*Electronic address: johan.gustafson@sljus.lu.se
†Present address: Dept. Física, Universidad de Oviedo, Avda. Calvo Sotelo s/n, 33007 Oviedo, Spain.

[1] H. Over *et al.*, Science **287**, 1474 (2000).
[2] B. L. M. Hendriksen and J. W. M. Frenken, Phys. Rev. Lett. **89**, 046101 (2002).
[3] S. Surnev *et al.*, Phys. Rev. Lett. **87**, 086102 (2001).
[4] M. Todorova *et al.*, Phys. Rev. Lett. **89**, 096103 (2002).
[5] M. Todorova *et al.*, Surf. Sci. **541**, 101 (2003).
[6] K. Reuter and M. Scheffler, Phys. Rev. Lett. **90**, 046103 (2003).
[7] C. I. Carlisle *et al.*, Phys. Rev. Lett. **84**, 3899 (2000).
[8] E. Lundgren *et al.*, Phys. Rev. Lett. **88**, 246103 (2002).
[9] W. X. Li, C. Stampfl, and M. Scheffler, Phys. Rev. Lett. **90**, 256102 (2003).
[10] K. Reuter and M. Scheffler, Appl. Phys. A **78**, 793 (2004).
[11] R. Nyholm *et al.*, Nucl. Instrum. Methods Phys. Res., Sect. A **467**, 520 (2001).
[12] S. Ferrer and F. Comin, Rev. Sci. Instrum. **66**, 1674 (1995).
[13] G. Kresse and J. Furthmüller, Comput. Mater. Sci. **6**, 15 (1996).
[14] G. Kresse and D. Joubert, Phys. Rev. B **59**, 1758 (1998).
[15] J. P. Perdew *et al.*, Phys. Rev. B **46**, 6671 (1992).
[16] M. V. Ganduglia-Pirovano *et al.*, Phys. Rev. B **63**, 205415 (2001).
[17] K. Reuter *et al.*, Phys. Rev. B **65**, 165403 (2002).
[18] J. Tersoff and D. R. Hamann, Phys. Rev. B **31**, 805 (1985).
[19] K. Reuter and M. Scheffler, Phys. Rev. B **65**, 035406 (2002).
[20] D. R. Jennison *et al.*, Phys. Rev. B **59**, R15 605 (1999).